ELSEVIER

Thermochimica Acta 287 (1996) 13–23

thermochimica acta

Non-isothermal kinetics of decomposition of $AlNH_4(SO_4)_2.12H_2O$ by EGA–MS

M. Kamruddin *, P.K. Ajikumar, S. Dash, R. Krishnan, A.K. Tyagi, K. Krishan

Materials Science Division, Indira Gandhi Centre for Atomic Research, Kalpakkam 603 102, Tamil Nadu, India

Received 31 January 1996; accepted 20 March 1996

Abstract

Real-time multiple-ion detection trend analysis mass spectrometry has been employed to study the temperature-programmed decomposition of $AlNH_4(SO_4)_2.12H_2O$ in the temperature range 300–1200 K. Significant correlations are established with certain non-isothermal solid state kinetic rate expressions through the use of fraction release plots obtained from Evolved Gas Analysis Mass Spectra (EGA–MS). The EGA mass spectra clearly resolve the dehydration stage and various other stages associated with the thermal decomposition. The dehydration step is concomitant with stage I of a three-stage ammonia release followed by the final decomposition of $Al_2(SO_4)_3$. These stages are found to comply with models based on random nucleation and diffusion approaches. A change in rate-governing mechanism was noticed with increase in the heating rate for the dehydration step. Relevant Arrhenius parameters such as the activation energy and pre-exponential factor were determined for all the decomposition stages. The ultimate product resulting from the decomposition was confirmed as γ-alumina by X-ray diffraction studies.

Keywords: Activation energy; Diffusion; Evolved gas analysis; Mass spectrometry; Solid state kinetics; Thermal decomposition

1. Introduction

Knowledge of single-particle kinetics is important for conducting solid-state calcination reactions under optimum conditions. Pertinent kinetic rate expressions can be

* Corresponding author.

PII: S0040-6031(96)02986-3

arrived at through mass spectrometric study of the time-dependent release behaviour of gaseous products from thermally ramped specimens. Non-isothermal techniques, especially temperature programmed ones, are used to obtain various Arrhenius parameters such as the activation energy, pre-exponential factors and appropriate kinetic rate expressions. Evolved Gas Analysis (EGA) refers to a host of techniques which monitor the concentrations of gases as functions of time while the specimen is subjected to programmed temperature control [1]. The EGA technique based on mass spectrometry [2,3] has significant advantages in terms of high sensitivity, specificity, fast response and multichannel detection capability. In this context, mass-spectrometry-based Evolved Gas Analyser (EGA–MS) has been built in our laboratory [4] for studying the temperature programmed decomposition of inorganic solids. γ-Al_2O_3 resulting from the vacuum thermal decomposition of $AlNH_4(SO_4)_2.12H_2O$, constitutes an important base material in a large number of catalytic and pharmaceutical preparations due to its high adsorptive power. The temperature programmed decomposition of $AlNH_4(SO_4)_2.12H_2O$ has been studied using the above facility. The real-time mass spectrometric data obtained in the temperature range 300–1200 K were used to construct EGA plots. The extent of fractional decomposition (α) evaluated from the EGA spectra was used to assess the integral form $g(\alpha)$ of various non-isothermal solid state kinetic equation models through suitable correlation. Various stages of decomposition revealed compliance with diffusion and random nucleation based models. In this paper, the experimental facility and kinetic results pertaining to the thermal decomposition of $AlNH_4(SO_4)_2.12H_2O$ along with the heating rate and the sample mass effect are described.

2. Experimental

A schematic diagram of the EGA–MS facility [4] is given in Fig. 1. Here, a high-temperature high-vacuum compatible quartz reaction chamber, evacuable to a pressure of 10^{-10} bar by a turbomolecular pumping system (TSU 330, Balzers, Germany) is coupled to an ultrahigh vacuum chamber through a variable conductance molecular leak valve (MD7, VG Micromass, UK). This reaction chamber is equipped with a membrane manometer (Membranovac MV 110 S2, Leybold SA, France) and micrometering valves for furnace atmosphere pressure control. The all-metal Ultra High Vacuum (UHV) chamber is pumped by another similar turbomolecular pumping system and a triode sputter ion pump (IZ 270, Leybold-Hereaus, Germany) to a base pressure of 3.0×10^{-13} bar. In addition to the quadrupole mass spectrometer (Dataquad, Spectramass, UK), the UHV chamber is equipped with other vacuum metrological hardware, including a magnetron gauge (IKR 020, Balzers, Germany), a spinning rotor viscosity gauge (SRG-2, MKS Instruments, USA) and calibration gas inlets.

In the present study, commercial analytical grade alum in powder form was used without any further treatment. In general, 100 mg of the sample was used except in the experimental runs where the effect of sample mass was investigated. The samples were heated in the quartz chamber at heating rates ranging from 3 to 14 K min^{-1}, using

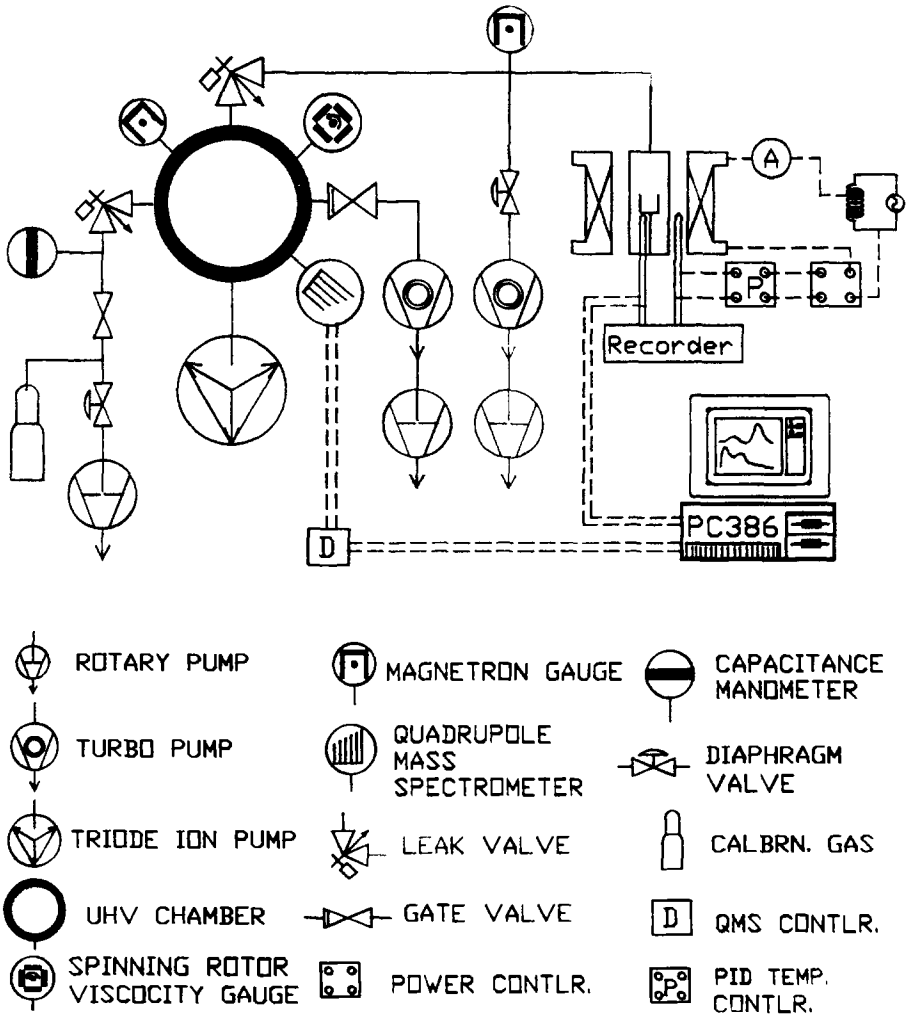

Fig. 1. The evolved gas analysis facility.

a programmable temperature controller (Eurotherm 906S, UK) in conjunction with a thyristor-controlled power supply. Two calibrated K-type Chromel–Alumel (Degussa AG, Germany) thermocouples were used to control and record the furnace and sample temperatures. A multi-pen strip chart recorder (R306M3, Rikadenki, Japan) was used to track temperature and other process parameters.

PC-based software has been developed [5] for obtaining temperature programmed multiple-ion detection real-time trend analysis mass spectra over a wide dynamic pressure regime. The software was designed to track ion intensities of 8 different masses (m/z) quasi-simultaneously through the RS232C interface of the quadrupole mass spectrometer. The ion intensities of H_2O^+ ($m/z = 18$), NH_3^+ ($m/z = 17$),

SO^+ ($m/z = 48$) and SO_2^+ ($m/z = 64$) were recorded in the temperature range 300–1200 K. In the case of NH_3^+, signal tracking took place after subtracting the OH^+ contribution. Between each successive experimental runs, hot inert gas purging was applied to avoid capillary condensation. The system was calibrated by leaking known quantities of gas into the UHV chamber through a molecular leak valve. The resulting rise in intensities of the quadrupole mass spectrometer was standardised against absolute pressure measurements by a Spinning Rotor Viscosity Gauge. The temperature- dependent multichannel trend analysis spectra were constructed by plotting ion intensities against the rising temperature signal tracked by a PC-based thermocouple add-on card.

3. Results and discussion

A typical EGA–MS plot of the temperature-programmed decomposition of $AlNH_4(SO_4)_2.12H_2O$ at a heating rate of 6 K min^{-1} in the temperature range of 300–1200 K is shown in Fig. 2. The dehydration of the sample under vacuum, as seen in the EGA–MS plot, occurs in the temperature range 300–500 K, whereas ammonia release occurs in three different stages. In stage I, ammonia release is concomitant with dehydration, whereas the stage II occurs in the temperature range 530–690 K. Stage III refers to a minor release peak around 700 K which signals the onset of decomposition of aluminium sulphate. The decomposition of alum yields γ-Al_2O_3 and SO_3, with the SO_3

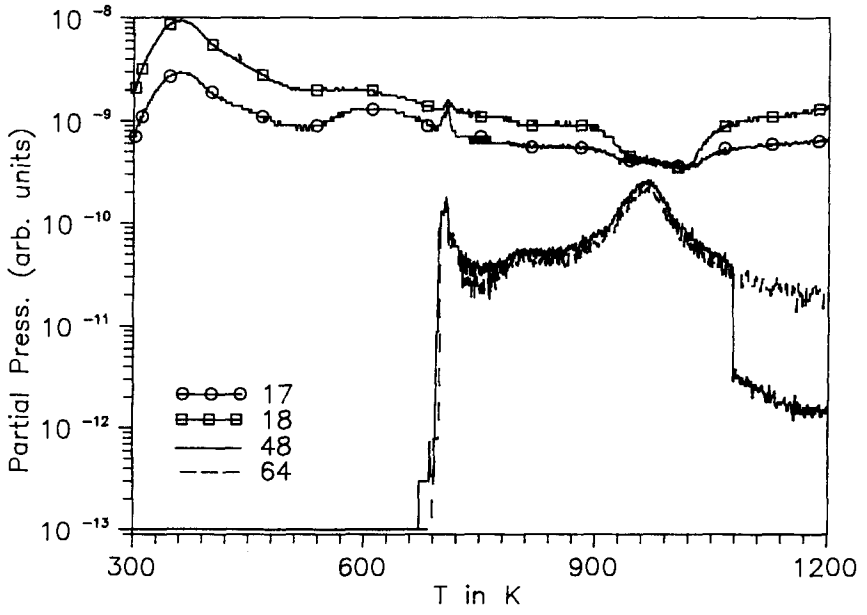

Fig. 2. EGA spectra for thermal decomposition of $AlNH_4(SO_4)_2.12H_2O$: sample mass, 100 mg; heating rate, 6 K min^{-1}

further decomposing to SO_2 and $\frac{1}{2}O_2$. The decomposition product SO_3 was not detected in our experiment by the mass spectrometer, perhaps due to its thermodynamic instability in an oxygen-deficient high-temperature environment [6]. The ion SO_2^+ was detected, along with its fragments formed by electron impact ionisation in the ion source of the quadrupole mass spectrometer. The intensities of ions SO^+ and $SO_2{}^+$ are depicted in the EGA plot of Fig. 2.

The three-stage decomposition sequence shown in the EGA–MS plot of Fig. 2 is in agreement with the reported thermogravimetric data on the same alum [7]. This corresponds to the evolution of 1 mole of SO_3 at 710 K, another mole at 800 K and the remaining two moles at 950 K.

For the purpose of evaluating the appropriate rate expressions governing the various stages of reaction, the fractional extent of decomposition α was evaluated from the EGA plot in the following manner (shown in Fig. 3)

$$\alpha(T) = A_{(T)}/A_{(\mathrm{TOTAL})}$$

where $\alpha(T)$ is fractional extent of reaction at temperature T, $A_{(\mathrm{TOTAL})}$ is total peak area, and $A_{(T)}$ the peak area covered up to temperature T.

The fractional extent of reaction (α) vs. temperature plots evaluated using this procedure for the dehydration and various stages of decomposition of $AlNH_4(SO_4)_2.12H_2O$ are given in Fig. 4.

We have used the integral forms of the non-isothermal kinetic expressions for evaluating the α–T values obtained from our EGA–MS data. Table 1 gives a list of the

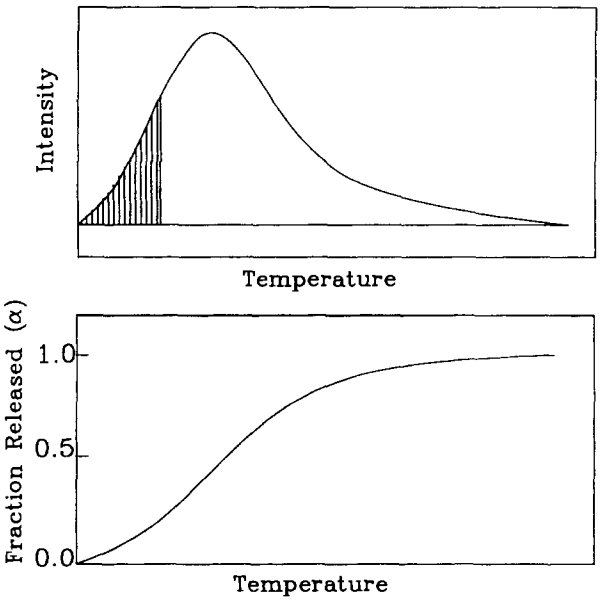

Fig. 3. Calculation of fractional extent of reaction (α). (a) Model trend analysis mass spectra. (b) Fractional reaction plot.

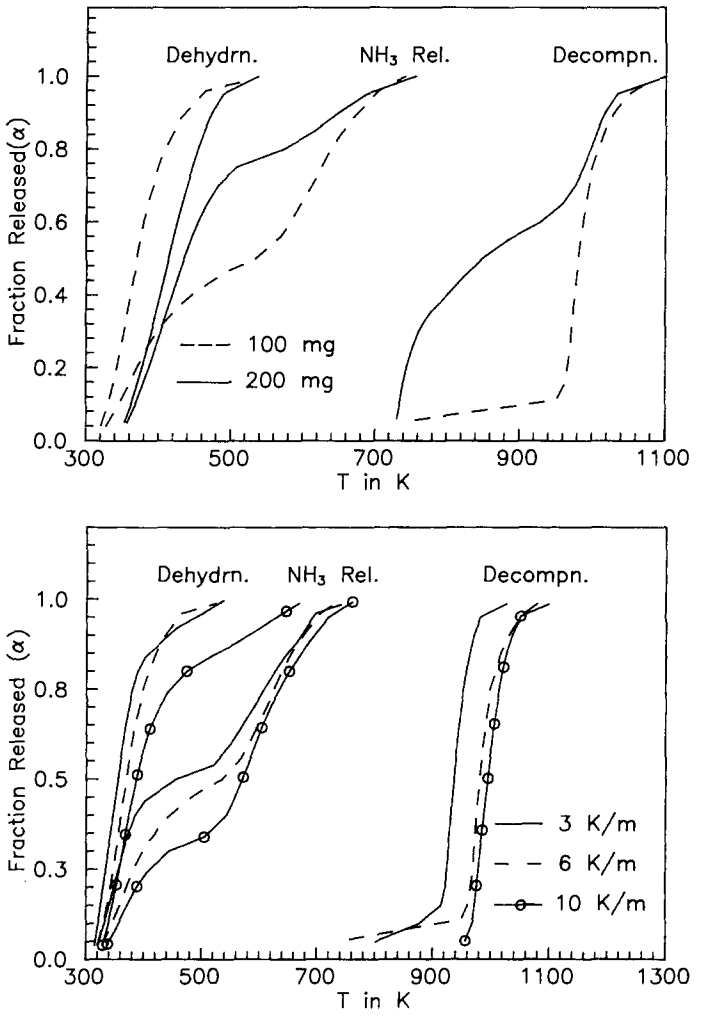

Fig. 4. Fractional reaction (α) vs. T plot for $AlNH_4(SO_4)_2.12H_2O$. (a) Showing sample mass effect. (b) Showing heating rate effect.

expressions used extensively for modelling gas–solid reactions [8] and Table 2 gives the best fits obtained for various stages of decomposition at different heating rates and the corresponding values of activation energies and pre-exponential factors.

It is evident that the best correlation for dehydration at lower heating rates was found with the Mampel unimolecular law formulated through random nucleation. In this approach, two-dimensional growth of randomly placed product nuclei in the form of edge-shaped planar circular discs proceeds simultaneously with the uncovering of surface gaseous species by desorption [9]. However, we have observed a change in the reaction mechanism governing the dehydration process with a change in heating rate

Table 1
Non-isothermal, integral forms of kinetic expressions for heterogeneous solid-state reactions

Rate-determining mechanism	Symbol	$f(\alpha)$	$g(\alpha) = \int_0^\alpha d(\alpha)/f(\alpha)$
		Nucleation and growth models	
Random nucleation approach			
(i) Mampel unimolecular law	A1	$1-\alpha$	$-\ln(1-\alpha)$
(ii) Avrami–Erofeev nuclei growth:			
(a) 2-Dimensional growth	A2	$2(1-\alpha)[-\ln(1-\alpha)]^{1/2}$	$[-\ln(1-\alpha)]^{1/2}$
(b) 3-Dimensional growth	A3	$3(1-\alpha)[-\ln(1-\alpha)]^{2/3}$	$[-\ln(1-\alpha)]^{1/3}$
(iii) Branching nuclei: Prout–Tompkins branching nuclei	A4	$\alpha(1-\alpha)$	$\ln[\alpha/(1-\alpha)]$
		Decelerating rate equations based on diffusion	
(i) Parabolic law, 1-dimensional transport	D1	α^{-1}	$\alpha^2/2$
(ii) 2-Dimensional diffusion	D2	$[-\ln(1-\alpha)]^{-1}$	$(1-\alpha)[\ln(1-\alpha)]+\alpha$
(iii) 3-Dimensional diffusion (Jander)	D3	$(1-\alpha)^{1/3}[(1-\alpha)^{-1/3}-1]^{-1}$	$1.5[1-(1-\alpha)^{1/3}]^2$
(iv) 3-Dimensional diffusion (Ginstling–Brounshtein)	D4	$[(1-\alpha)^{-1/3}-1]^{-1}$	$1.5[1-2\alpha/3-(1-\alpha)^{2/3}]$
		Phase boundary movement	
(i) 1-Dimensional (zero-order)	R1	Constant	α
(ii) 2-Dimensional (cylindrical symmetry)	R2	$(1-\alpha)^{1/2}$	$2[1-(1-\alpha)^{1/2}]$
(iii) 3-Dimensional (spherical symmetry)	R3	$(1-\alpha)^{2/3}$	$3[1-(1-\alpha)^{1/3}]$

(Table 2). At higher heating rates, the diffusion limitations predominate over random nucleation. The experimental data at 10 K min^{-1} showed better correlation with the Jander rate expression based on three-dimensional diffusion. The diffusion-limited behaviour is attributable to thermal-gradient-driven mass transfer effects specific with higher heating rates.

The sample shows multiple stages of ammonia release. This corresponds to varying degrees of thermal stability associated with non-equivalent crystallographic location of ammonium ions in the basic alum structure. The stage I ammonia release data show consistent correlations with the three-dimensional diffusion approach based on the Jander formalism. The reason for this can be ascribed to a progressive build-up of barrier layers of intermediate products which need to be permeated for gas release. The higher E value at 14 K min^{-1} is due to a larger overlap of stage-II release which was not completely resolved. The stage-II ammonia release shows compliance with rate expressions based on the Brounshtein mechanism propounded on the basis of three-dimensional diffusion. However, this model, unlike the Jander approach, accounts for the difference between reactant and product molar volumes. As substantial volume

Table 2
Reaction mechanism, corresponding correlation coefficients, activation energy and pre-exponential factors for various stages of decomposition of $AlNH_4(SO_4)_2.12H_2O$ at different heating rates

Heating rate/ K min^{-1}	Mechanism	Correlation coefficient	Activation energy kJ mol^{-1}	Pre-exponential factor/s^{-1}
			Dehydration	
3	Al	0.986	29.27	18.3
6	Al	0.983	27.3	8.7
10	D3	0.976	37.6	29.6
14	D3	0.969	42.09	18.8
			NH_3 release : stage I	
3	D3	0.986	45.52	1.2×10^{2}
6	D3	0.96	17.36	4.0×10^{-3}
10	D3	0.95	28.32	0.1
14	D3	0.99	47.27	66.5
			NH_3 release : stage II	
3	D2	0.996	16.1	2.6×10^{-3}
3	D4	0.995	18.4	1.8×10^{-3}
6	D2	0.996	25.5	4.3×10^{-2}
6	D4	0.998	30.46	5.1×10^{-2}
10	D2	0.992	32.00	0.26
10	D4	0.993	35.27	2.1
			Decomposition	
3	Al	0.986	269.95	1.5×10^{12}
6	Al	0.97	321.58	1.7×10^{14}
10	Al	0.986	323.84	4.7×10^{14}
14	Al	0.98	187.0	5.1×10^{6}

changes occur during stage-II ammonia release leading to formation of $Al_2(SO_4)_3$, this mechanism prevails. Stage-II ammonia release also correlates well with two-dimensional diffusion control. This is clearly an indication of the appearance of active surfaces created by disruptive effects on the crystal structure. As stage III is accompanied by a burst of residual ammonia over a short temperature range, separate kinetics could not be evaluated.

The final stage of decomposition, which leads to the formation of γ-Al_2O_3, is again governed by random nucleation, a process closely controlled by surface desorption of gases from finely dispersed crystallites. The estimated activation energies match well with the values obtained by Johnson et al. [10] in their isothermal runs.

The effects of sample mass and heating rates on the fractional extent of decomposition have been investigated. Typical results are shown in Fig. 4. Plots of the various stages of decomposition for 100 and 200 mg sample mass, respectively, at a heating rate of 6 K min^{-1} are shown in Fig. 4a. The dehydration stage is controlled by random nucleation, a phenomen on essentially based on surface desorption, but it does not lead to a change in the slope of the α–Tcurves. However, a shift of the curve towards high temperature is seen. This can be attributed to temperature gradients in the sample.

Unlike dehydration, α-T curves for ammonia release, as well as the decomposition stages, show change in the slope. Thermal inertia and product layer formation leading to diffusional limitations in gas release contribute to the decrease in the slope of these curves. Fig. 4b shows the heating rate effect on α-Tcurves obtained for a 100 mg sample at typical rates of 3, 6 and 10 K min^{-1}. With increasing heating rates, the peak release temperature increases. This is again attributed to heat transfer effects arising from thermal gradients in the sample.

X-ray powder diffraction studies were carried out on the initial alum sample as well as on the residue material left after each decomposition regime. The results are shown in Fig. 5. It can be seen that the extensively hydrogen-bonded initial alum, having an

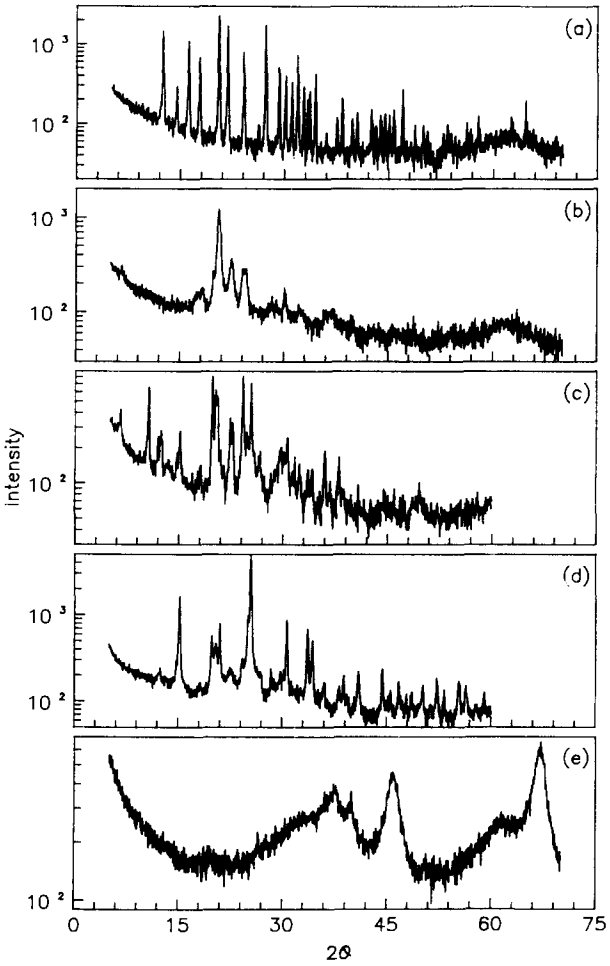

Fig. 5. X-ray diffractogram of: (a) original alum sample; (b) amorphised sample after dehydration and stage I ammonia release; (c) recrystallised intermediate; (d) structure preceding formation of γ-Al_2O_3; (e) final product γ-Al_2O_3.

Alunite superstructure [11] containing an NH_4^+ cation and SO_4^{2-} anion substructure, shows multiple reflection lines in the powder X-ray diffractogram, Fig. 5a. However, the X-ray diffractogram taken after dehydration and stage-I ammonia release, Fig. 5b, indicates total collapse of the crystal structure, probably due to the disappearance of hydrogen bonding. At temperatures above 500 K, the formation of a recrystallised intermediate structure results in the numerous Bragg diffraction lines shown in the diffractogram of Fig. 5c. With increasing temperature, a progressively simplified unit cell is obtained as inferred from the fewer Bragg peaks seen in Fig. 5d. On complete decomposition, γ-Al_2O_3 with a defect spinel structure is obtained, Fig. 5e. Formation of finely dispersed γ-Al_2O_3 crystallites is a consequence of total collapse of the original Alunite structure of the alum. This is confirmed by the X-ray diffraction data.

4. Conclusion

A Quadrupole Mass Spectrometry based Evolved Gas Analysis facility has been used to study the temperature programmed decomposition of $AlNH_4(SO_4)_2.12H_2O$. Concurrent steps such as dehydration and ammonia release could be successfully resolved. Reaction mechanisms governing various stages of decomposition have been identified. Possible explanations for the observed change in mechanisms for dehydration at higher heating rates are given. The activation energies obtained for dehydration, two ammonia release stages and the decomposition stage at 6 K min^{-1} are 27.3, 17.36, 27.0 and 321.6 kJ mol^{-1} respectively. The final structure, γ-Al_2O_3, resulting from decomposition of the sample was confirmed by X-ray powder diffraction.

Acknowledgements

The authors duly acknowledge K. Govindarajan for providing the high purity material. We also acknowledge B. Purniah for instrumentation support. We thank J. Janaki for useful discussions and G.V.N. Rao for acquisition of X-ray powder diffraction patterns.

References

[1] H.G. Langer, in P.J. Elving (Ed), Treatise on Analytical Chemistry, Part I, Vol. 12, John Wiley & Sons, New York, 2nd edn., 1983. p. 229.
[2] D. Price, D. Dollimore, N.S. Fatemi and R. Whitehead, Thermochim. Acta, 42 (1980) 323.
[3] D. Price, N.S. Fatemi, D. Dollimore and R. Whitehead, Thermochim. Acta, 94 (1985) 313.
[4] M. Kamruddin, P.K. Ajikumar, S. Dash, B. Purniah, A.K. Tyagi and K. Krishan, Instrum. Sci. Technol., 23 (2) (1995) 123.
[5] N. Saraswathy, Control and Data Acquisition of Quadrupole Mass Analyser, Project Report, University of Madras, 1994.
[6] T. Leskela, M. Lippmaa, L. Niinisto and P. Soininen, Thermochim. Acta, 214 (1993) 9.

[7] P.J. Pizzolato and H.A. Papazian, J. Am. Ceram. Soc., 53 (5) (1970) 289.
[8] C.H. Bamford and C.F.H. Tipper (Eds.), Comprehensive Chemical Kinetics, Vol. 22, Reactions in the Solid State, Elsevier, Amsterdam, 1980, p. 41.
[9] H. Tanaka and N. Koga, J. Chem. Ed., 72 (3) (1995) 251.
[10] D.W. Johnson, Jr., and P.K. Gallagher, J. Am. Ceram. Soc., 54 (9) (1971) 461.
[11] T.C.W. Mak and Gong-Du Zhou, Crystallography in Modern Chemistry: a Resource Book of Crystal Structures, John Wiley & Sons, New York, 1992, p. 277.